Fall 2010

Resistance switching in electrodeposited magnetite thin films

Samantha Glen Matthews

Department:

RESISTANCE SWITCHING IN ELECTRODEPOSITED MAGNETITE THIN FILMS

by

SAMANTHA GLEN MATTHEWS

A THESIS

Presented to the Faculty of the Graduate School of the

MISSOURI UNIVERSITY OF SCIENCE AND TECHNOLOGY

In Partial Fulfillment of the Requirements for the Degree

MASTER OF SCIENCE IN MATERIALS SCIENCE & ENGINEERING

2010

Approved by

Jay A. Switzer, Advisor
Richard K. Brow
Julia E. Medvedeva

ABSTRACT

The resistance switching phenomenon has been extensively studied in metal oxide thin films for its applications in the non-volatile memory industry. The research presented here focuses on magnetite thin films which have been electrodeposited onto gold-sputtered glass substrates via the electrochemical reduction of a Fe(III)-triethanolamine complex in aqueous alkaline solution. Magnetite was chosen for its usefulness in read/write memory applications, its high Curie temperature, its metal-to-insulator (Verwey) transition, and its half-metallic character and attendant spintronic properties. Resistance switching behavior caused by a reversible redox reaction at the anode was observed in the films, demonstrating that electrodeposited films show the same characteristic behavior observed in films deposited via other methods. Electrochemical methods, as well as scanning electron microscopy and X-ray diffraction, were used to characterize the films.

ACKNOWLEDGMENTS

I would like to take the opportunity to thank my advisor, Dr. Jay Switzer, for his patience and support over the last two years, and for the opportunity to enter the wide world of materials engineering.

I would also like to thank my committee members, Dr. Richard Brow and Dr. Julia Medvedeva, for giving so generously of their time and expertise.

I'm grateful to my group members, Beth Kulp, Rakesh Gudavarthy, Zhen He, Guojun Mu, Niharika Burla, and Andrew Wessel, for working alongside me and being willing to help out a non-chemist. In particular, Beth was always ready with kindness and assistance, and Andrew with morale-boosting conversations about *Doctor Who* and Comic-Con. In addition, Dr. Eric Bohannan was there to provide friendly words and his XRD prowess.

Dr. Greg Hilmas and Dr. Wayne Huebner provided encouragement and guidance far beyond what was required, and their excellent leadership helped make the Ceramic Engineering department feel like home. Denise Eddings assisted with her warmth and her knowledge of the labyrinthine world of graduate regulations.

My parents, Dean and Judith Matthews, never wavered in their belief in me, and that, perhaps more than anything else, kept me going when things got difficult.

Finally, the encouragement I've received from my friends has been invaluable. Rachel Day, Jacob Balson, Martha Cameron and Josh Holzhausen gave me their strength when I had none left of my own. Without them, I never would have finished.

TABLE OF CONTENTS

LIST OF ILLUSTRATIONS

1. INTRODUCTION

The semiconductor industry has long required a high-density, high-speed and low-power memory technology that retains its data even if the power is interrupted [1]. As device features approach the sub-100 nm regime, the semiconductor industry is having trouble keeping up [2]. Materials with reversible resistance switching at room temperature have become more and more attractive because of their very low power consumption, quick switching speed, and non-destructive readouts. While static RAM (SRAM) and dynamic RAM (DRAM) are very fast, they are both volatile, which costs energy and additional circuitry. Traditional non-volatile Flash memory based on charge storage is quickly approaching its scaling limit due to the increasing difficulty of retaining electrons in shrinking dimensions. It is also slow (write time > 1 μs). Likewise, magnetic RAM (MRAM) and ferroelectric RAM (FRAM) have severe scaling problems. Resistance switching RAM (RRAM), which is based upon resistance change modulated by electrical stimulus, has speed, scalability, and multibit storage potential [1, 3-4]. The reading of resistance states is non-destructive, and the memory devices can be operated without requiring transistors in every cell, making a cross-bar structure feasible [5-6]. Resistance switching programming speeds have surpassed DRAM, matched SRAM, and outstripped other new memory technologies like phase-change memory or molecular memory [6-9].

Many solid-state materials show resistance switching characteristics, including binary transition metal oxides. These have simple compositions and show resistance switching in polycrystalline states, minimizing the requirements for deposition techniques, temperatures and substrates. It is therefore possible to use conventional industrial techniques at low temperatures to fabricate high-performance resistive memory, which is promising for manufacturing and 3D stacking.

Metal-insulator-metal systems display electrically-induced resistance switching phenomena and have thus been proposed as the basis for non-volatile computer memory. They unite the benefits of Flash and DRAM (dynamic random access memory) while eliminating their drawbacks, and they have the potential to be highly scalable.

Fe_3O_4 has a much simpler crystallographic structure than many of the other candidate materials, making it easier both to model and to prepare experimentally. It also has a long history of technological use, so that its preparation and characteristics are well-documented, and it can be grown with only minor modifications to existing techniques.

2. REVIEW OF LITERATURE

2.1. BACKGROUND

Half-metallic ferromagnets have stirred up much theoretical and practical interest since de Groot first predicted their existence based on band structure calculations of NiMnSb [10]. By definition, half-metallic ferromagnets have metallic character for one electron spin population and insulating or semiconducting character for the other. They therefore have 100% spin polarization of the conduction band. Much of the interest in these materials comes from the potential use of half-metals as pure spin sources in spintronic devices which would exploit the electron's spin state as well as its charge to make non-volatile, radiation-hard data processing and storage devices [11].

At room temperature, magnetite has a cubic inverse spinel structure, illustrated in Figure 2.1, in which the larger O ions make up a close-packed fcc structure, with the smaller Fe ions occupying two different interstitial sites within the oxygen lattice that are denoted as A and B. A third of the Fe ions occupy the tetrahedrally-coordinated A sites, which consist only of Fe^{3+} ions, while the other two-thirds occupy the B sites. The B sites are octahedrally coordinated and consist of both Fe^{2+} and Fe^{3+} ions in a random distribution. From the Verwey transition at 120 K to the Curie temperature at 860 K, the moments within the discrete A and B sublattices are anti-ferromagnetically coupled; that is, ferromagnetically coupled, but in opposite directions. The spins on A are antiparallel to the spins of the B sublattice, resulting in a negative AB exchange and a net magnetic moment from the B site Fe^{2+} ions. This gives an overall ferrimagnetic character with a net magnetic moment of 4.1 μ_B per formula unit [12]. The theoretical local spin density approximation band structure calculations for this ferrimagnetic phase predict that it is half-metallic with a spin-up band gap of ~0.4 eV and a partially filled metallic spin-down t_{2g} conduction band [13]. Magnetite is a material of interest for magnetic memory and spin-dependent transport because it has a calculated spin polarization of 100% at the Fermi level [14-15]. Negative spin polarization has also been experimentally confirmed [16-18].

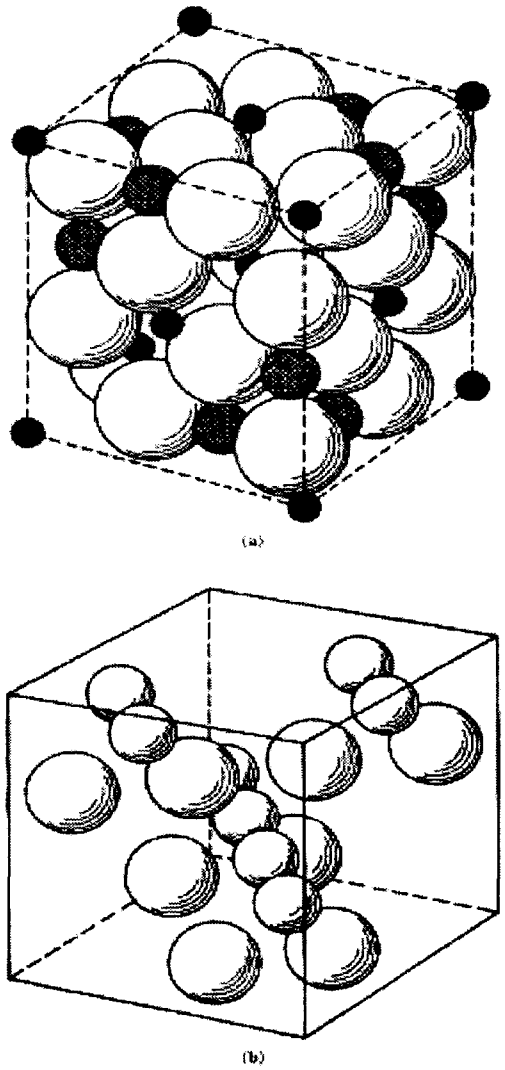

Figure 2.1. The structure of magnetite. a) shows the structure above T_V, with the large spheres denoting oxygen ions, the black spheres Fe^{3+} ions in the tetrahedral sites, and the cross-hatched spheres Fe^{3+} and Fe^{2+} ions in the octahedral sites. b) shows the structure below T_V, with the large spheres denoting Fe^{2+} ions and the small spheres Fe^{3+} ions. [18]

Fe_3O_4 undergoes a Verwey transition at 120 K which is marked by a sudden drop in conductivity by two orders of magnitude upon cooling through the transition, along with a sharp drop in magnetization. Verwey and Haayman interpreted this as stemming from spontaneous charge ordering of the Fe B lattice sites, which causes a structural shift from cubic to monoclinic, and the cessation of the two-stage electron hopping process

between the 2+ and 3+ B lattice sites that is the primary conduction mechanism above T_v [19].

Since the first report on oxide insulators by Hickmott in 1962 [20], hysteretic resistance switching has been observed in a great many materials in a metal-insulator-metal (MIM) configuration. There was a great deal of research into the phenomenon up through the mid-1980s [21-23], with a second wave starting in the late 90s, initiated by Asamitsu, Kozicki and Beck [24-26].

Both nanocrystals and single-crystal thin films display strong electrically driven hysteretic switching of electronic conductance once sample temperatures are lowered below T_V. The transition is caused not by local heating above T_V, but by an electrically driven breakdown of the insulating state. While qualitatively similar resistance switching has been seen in other correlated oxides [27-28], the switching in magnetite is a bulk effect with a distinct mechanism [29].

Since RRAM memory has a simple structure, highly scalable cross-point and multilevel stacking memory structures have been suggested. In the resistance switching phenomenon, a large change in resistance occurs when pulsed voltage is applied, and the resistance of the cell can be set to a desired value by applying the correct voltage pulse [30]. The switching speed can be less than several ns [31].

There are two classifications with regard to the electrical polarity needed for resistively switching MIM systems. The switching is known as unipolar (or symmetric) when the switching does not depend on the polarity of the voltage and current signal. The switching is bipolar (or antisymmetric) when the set to an on state occurs at one voltage polarity and the reset to the off state occurs at reversed voltage polarity. The structure of the system has to have some asymmetry—such as differing electrode materials or the voltage polarity during the initial electroforming step—to display bipolar switching behavior. For both unipolar and bipolar resistance switching, reading of the state is performed at voltages which are small enough not to affect the state. The differing switching characteristics can be seen in Figure 2.2.

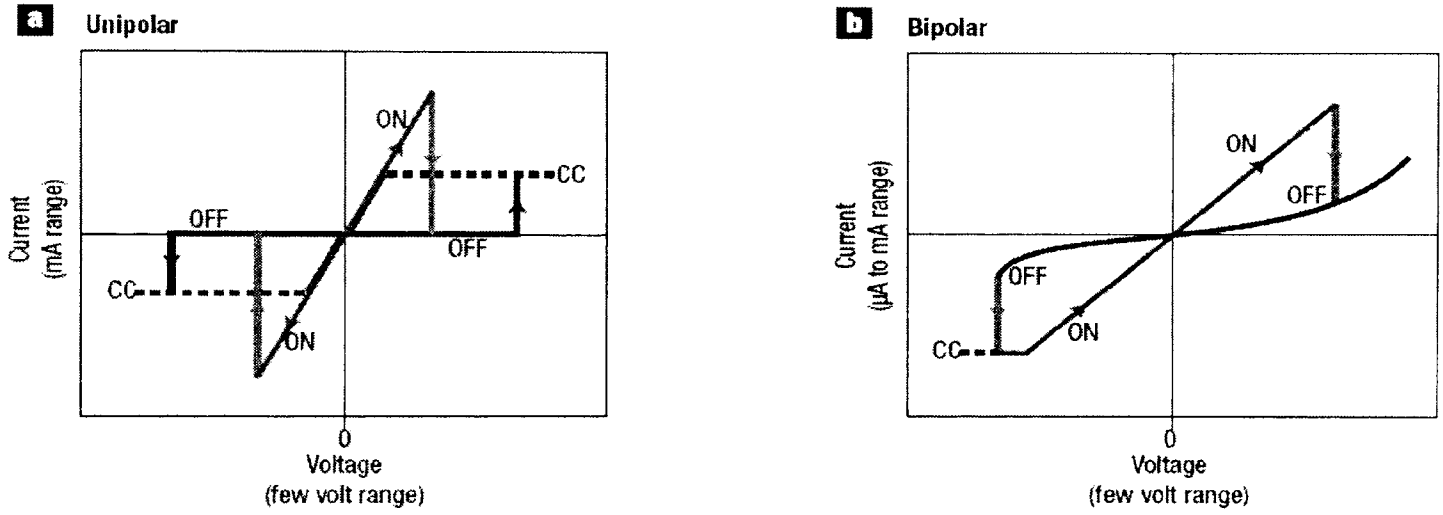

Figure 2.2. The two types of resistance switching. a) illustrates unipolar switching while b) shows bipolar switching. CC denotes compliance current. [32]

Theoretical mechanisms for resistance switching in MIM regimes are often comprised of a mixture of physical and chemical effects. However, the mechanisms can be broadly sorted according to whether their dominant contribution comes from a thermal, electronic, or ionic effect.

Resistance switching driven by a thermal effect is unipolar. It is triggered by a voltage-induced partial dielectric breakdown in which the material in a discharge filament is modified by Joule heating. During the reset transition, the conducting filament is again disturbed thermally by the high local power density generated, on the order of 10^{12} W/cm^3. A critical variable for unipolar switching appears to be the value of the compliance current. For instance, it has been shown that a TiO_2 thin film displays bipolar resistance switching and that this can be changed to unipolar switching by increasing the value of the compliance current [32].

Another possible source of resistance switching is electronic charge injection and/or charge displacement effects. The charge-trap model is one option, in which charges are injected by Fowler-Nordheim tunneling in high electric fields and then trapped at sites such as defects or metal nanoparticles in the insulator [33]. This changes

the electrostatic barrier attributes of the MIM structure and therefore its resistance. In a slightly different model, the trapping at interface sites is believed to modify the adjacent Schottky barrier at various metal/semiconducting perovskite interfaces [34-36].

Yet another possibility is the insulator-metal transition (IMT), in which electronic charge injection mimics doping to induce an IMT in perovskite-type oxides. This model has recently been extended to bipolar switching [37].

Finally, a ferroelectric model has been proposed by Esaki [38] and described by Kohlstedt et al [39]. In this model, an ultrathin ferroelectric insulator is assumed whose ferroelectric polarization direction modifies the tunneling current through the insulator.

Bipolar resistance switching connects nanoelectronics to nanoionics since ionic transport and electrochemical redox reactions drive the mechanism. One class of resistance switching behavior relies on the formation of conductive filaments in the on state on the cell; when the polarity of the applied voltage is reversed, the filaments are electrochemically dissolved, resetting the system to its off state. A second class relies upon the migration of anions (usually oxygen ions) towards the anode, a resultant stoichiometry change, and a valence change of the cation sublattice associated with a modified electronic conductivity.

Faraday's studies of Ag_2S established the thermodynamical theory of ionic conduction that is characteristic of a solid electrolyte [40]. By using solid electrolytes in which conduction is due to metal cations, the creation and destruction of a metal filament in the MIM system can be controlled. Since the chemical reaction ideally doesn't damage the MIM system, the switch will, in theory, work indefinitely [41].

Since the switching bias voltage is mainly determined by the activation energy for the chemical reaction and the ionic diffusion constant, the operating bias voltage can be adjusted via the choice of materials for the MIM system, especially the ion-conducting material.

In many oxides, especially transition metal oxides, oxygen ion defects (usually oxygen vacancies) are much more mobile than cations. If the cathode blocks ion exchange reactions during the electroforming process, an oxygen-deficient region starts to form and expand toward the anode. Transition metal cations allow for this deficiency

by trapping electrons emitted from the cathode. The reduced valence states of the transition metal cations produced by this electrochemical process turn the oxide into a metallically conducting phase. This virtual cathode proceeds toward the anode and forms a conductive path [42]. Bipolar switching occurs via local redox reactions between the virtual cathode and anode by forming or breaking the conductive contact. Depending on the charge transfer during resistance switching, the resistance of the system can be set at an intermediate level, which may be useful for creating multibit storage in memory cells [43].

Many transition metal oxides display charge and orbital orderings which show themselves as a spatial localization of charge carriers on certain ionic states and electron orbitals, respectively. These related ordering processes determine the physical properties, such as charge transport and magnetism [44-46]. Magnetite is an important 3d transition metal oxide due to its half-metallic character, high Curie temperature (860 K), and the presence of a metal-insulator transition, known as the Verwey transition, at 120 K. This makes it a promising material for spintronic applications [47-49].

Despite much experimental and theoretical work, the actual mechanics of the electrical transport mechanism in magnetite are still unresolved. Fe_3O_4 experiences a first-order Verwey transition at T_v=120 K. Below the Verwey transition, there is a long-range order (LRO) of the Fe^{2+} valence electrons. At T_v the DC conductivity abruptly changes by a factor of about a hundred. Above T_v the DC conductivity increases noticeably with temperature and reaches a maximum at T_m=305 K [50-51].

Most of the proposed mechanisms are predicated on either the hopping or band motion of the valence electrons. All the prior quantitative descriptions of the electrical conductivity above T_v using the small polaron (SP) model start with interacting SP models and take their SP hopping conductivity to be the main conduction mechanism [52-56], but these explanations do not adequately explain the electrical conductivity.

The DC conductivity in the high-temperature phase of Fe_3O_4 can be explained by superimposing SP band and SP hopping conduction. Band conduction is the dominant transport mechanism below room temperature, while at 350 K both contributions are equal in magnitude. Above 350 K the SP band conductivity quickly decreases because of

the exponential decrease in t with temperature, and hopping conduction becomes dominant.

Resistive random access memory (RRAM) is based on resistance switching in materials such as transition metal oxides. Natelson's group showed that nanophase magnetite deposited via molecular-beam epitaxy displays resistance switching behavior; they attributed it to an electric field driven insulator-to-metal phase transition below the Verwey temperature of 120 K due to strong electron-phonon coupling [57-58]. Below the Verwey transition, magnetite is in a charge-ordered state with strong coupling of phonons to conduction electrons [59]. The applied electric field may break down the charge-ordered state in the material [60-62].

Since the driving mechanism for RRAM has not yet been entirely explained, its development has lagged behind that of other candidates for next-generation non-volatile memories, making understanding the driving mechanism a critical issue. The proposed models can be grouped into categories according to their switching behavior and conducting path.

For filamentary conduction, as in unipolar switching, thermal redox and/or anodization near the electrode/oxide interface is widely accepted as the mechanism responsible for the formation and rupture of the filaments [63-64]. Conversely, in bipolar switching, electrochemical migration of oxygen ions is considered to be the driving mechanism [65]. These mechanisms are illustrated in Figure 2.3, with a typical RRAM cell seen in Figure 2.4.

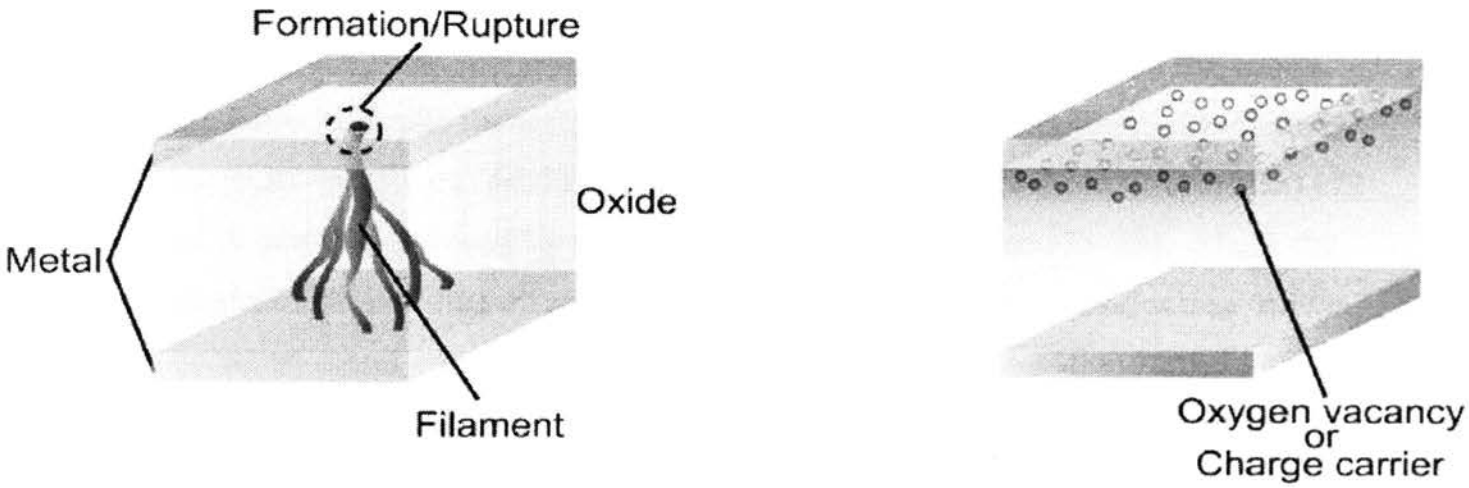

Figure 2.3. Filamentary vs. vacancy conduction. [61]

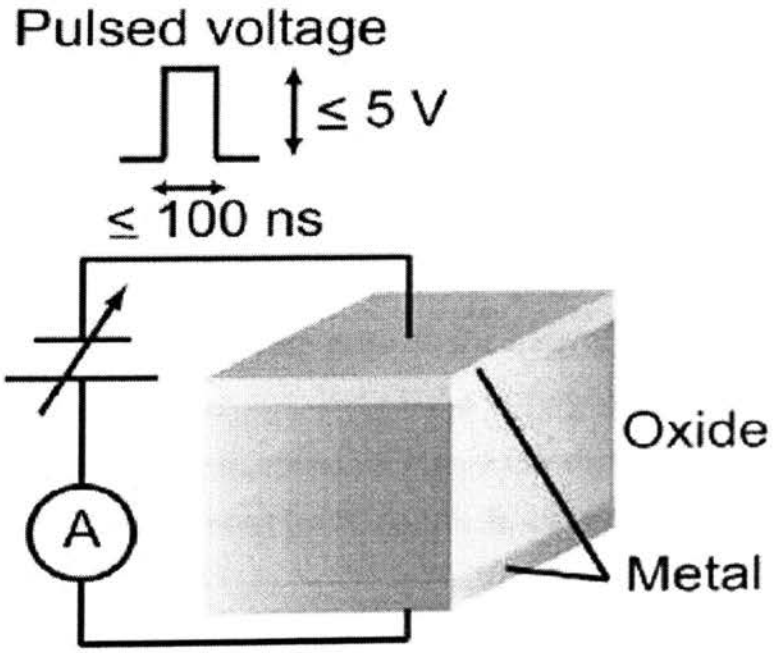

Figure 2.4. A typical RRAM cell. [61]

The other kind of conducting path is an interface-type path, in which the resistance switching occurs at the interface between the metal electrode and the oxide. Several models have been put forth for this type of switching, including electrochemical migration of oxygen vacancies [66-71], trapping of charge carriers (hole or electron) [72-74], and a Mott transition induced by carriers doped at the interface [75-78]. Since the memory cell has a capacitor-like structure made of insulating or semiconducting oxides sandwiched between metal electrodes, a Schottky barrier is the most likely origin of the contact resistance. The amplitude of the contact resistance is attributed to the potential profile of the barrier. For interface resistance switching, the switching characteristics should depend on the electronic properties at the interface. Studies have shown that modifying the electronic properties at the interface does indeed change the resistance switching behavior; the carrier concentration at the interface also plays an important role [79-80]. For example, oxidative treatment of RRAM cells has been demonstrated to modify their resistance switching properties [81].

Sawa's group cited the Schottky barrier effect between the metal (oxide) electrode and the insulator as the cause of resistance switching [82], so that the thin interface layer (less than a few nm) is responsible for rectifying resistance switching.

High-to-low resistance switching is driven by the application of high voltage, and the up-and-down sweeps of current-voltage (IV) characteristics often exhibit hysteresis (that is, the current does not retrace itself when the bias voltage is swept). For nanoscale magnetite, the low-resistance state only persists for a certain voltage interval; the system then returns to the high-resistance state before the voltage returns to zero. Although the high-to-low resistance switching in epitaxial magnetite thin films is driven by the applied electric field, the hysteresis observed in IV curves is caused by Joule heating in the low resistance state.

Resistance switching in magnetite occurs only below T_v, where magnetite is in a correlated ordered state [83]. This makes magnetite resistance switching a strong candidate for the theoretically predicted breakdown of charge-ordered states by electric field [84].

Most resistance switching materials show different resistance switching behaviors as the film thickness decreases, causing scaling problems. Process integration and compatibility are also very important considering that the current technological infrastructure is built around silicon CMOSs (complementary metal oxide semiconductors). A buffer layer is required to grow an epitaxial oxide on Si [85].

The biggest issues in the practical use of RRAM are data retention, memory endurance, and the variations among different cells and chips. A data retention time of over 10 years can be extrapolated from high-temperature measurements [86-88], while an endurance of 10^6 cycles has been seen in a NiO cell [89]. If borne out, these numbers would make RRAM an acceptable alternative to Flash memory, but a statistical study on reliability is still essential.

2.2. THEORY

For magnetite, the electron-electron interactions, electron-phonon interactions, and the electronic bandwidth are all of similar magnitude [90]. This results in electronic properties not seen in simpler materials with weak electron-electron interactions. Above the Verwey temperature, magnetite forms an inverse spinel structure AB_2O_4, with the tetrahedrally-coordinated A sites occupied by Fe^{3+} and the octahedral, mixed-valence B sites evenly split between Fe^{3+} and Fe^{2+} atoms. One explanation for the Verwey transition attributes high-temperature conducting to fluctuating valences of the B sites, with the transition arising from B-site charge ordering as the temperature decreases, and a simultaneous first-order structural phase transition to a monoclinic unit cell. However, the actual mechanism is under debate [91-92], with some researchers crediting the structural degrees of freedom as responsible for the change in conductivity [93-94]. Recent theoretical research has made strides in describing the complicated relationship between charge and structural degrees of freedom [95-96], including a model of the transition mechanism with strongly correlated $3d$ Fe electrons amplifying the electron-phonon couplings [97].

One of the mechanisms that affects the magnetotransport behavior of magnetite is its anisotropic magnetoresistance (AMR). In ferromagnetic materials, AMR is caused by

spin-orbit interaction, which results in the intermixing of spin-up and spin-down states [98-100]. This mixing depends on the magnetization direction and so causes a magnetization-direction-dependent scattering rate. Therefore, the conductivity of a saturated sample is affected by the angle between the electrical current **J** and magnetization **M**. The angular dependence is

$$\rho=\rho_{\perp}+(\rho_{\parallel}-\rho_{\perp})\cos^2\Theta \qquad (1)$$

where $\rho_{\parallel}$ and $\rho_{\perp}$ are the resistivities for $\mathbf{M} \parallel \mathbf{J}$ and $\mathbf{M} \perp \mathbf{J}$, respectively [101].

Various mechanisms have been put forward to explain the origin of AMR and its connection to spin-orbit coupling. In epitaxial thin films, additional AMR features are observed at low fields and are related to the magnetocrystalline anisotropy. The AMR shows a deviation of the angular dependence from the $\cos^2\Theta$ curve [102-103]. There is also an anomalous temperature dependence where the magnitude of AMR peaks at a temperature close to the Verwey transition. The cause of this anomaly is hotly debated [104-105].

The temperature dependence of resistivity in magnetite films suggests that electronic transport in magnetite is a thermally activated behavior. Three regions with different activation energies can be delineated [106]. The first is a high-temperature region ($T \geq 200$ K), the second is middle-temperature (just above T_v to ~200 K), and the third is low-temperature (below T_v), referred to as regions I, II and III, respectively. For mechanisms, small-polaron hopping

$$\rho/T^{3/2}=Ae^{(Wp/k_BT)} \qquad (2)$$

seems to fit well for I, Arrhenius law/band-gap model

$$\rho=\rho_{\infty}e^{(Ea/k_BT)} \qquad (3)$$

for II and III, and variable-range hopping

$$\rho=\rho_{\infty}e^{(T_0/T)(1/4)} \quad (4)$$

for temperatures below T_v [101]. The existence of two different electrical conduction regions above T_v (i.e. I and II) in magnetite agrees well with Ihle and Lorenz's model for small-polaron (SP) band and SP hopping conduction [107], with the first dominant at lower temperatures (II, just above T_v) and the latter at higher temperatures (I).

Piekarz et al. [108-109] proposed a mechanism for the Verwey transition as a cooperative effect between the intra-atomic Coulomb interaction of Fe ions and phonon-driven lattice instability. Their model shows that the strong electron-phonon coupling induces local crystal deformations and a polaronic short-range order above T_v; the signs of the Verwey transition already appear around 200 K [110-112]. According to them, the X_3 transversal optic phonon mode is responsible for the appearance of charge-order stabilization at temperatures above the Verwey transition. The charge ordering precipitates a charge disequilibrium between the B-site Fe ions (octahedrally coordinated cation sites in the spinel structure of magnetite), departing from the average $Fe^{+2.5}$ state to Fe^{+2} and Fe^{+3} at different octahedral sites. Thus, the charge ordering enhances the effect of the spin-orbit interactions.

Above the Verwey transition, magnetite has an inverse spinel structure due to an ordering of the ferrous and ferric ions in the octahedral interstices of the spinel lattice, which necessitates a transition to an orthorhombic structure [113]. From observations of the conductivity above and below the Verwey transition as well as of magnetically-induced anisotropy below T_v, it seems that the dominant conductivity mechanism in magnetite is that of electron hopping between the ferrous and ferric ions in the octahedral lattice sites. For the nucleation process required to initiate the growth of a conductive filament, the rate of critical nucleation is proportional to $e^{(const/\Delta\mu)}$, where $\Delta\mu$ is the change in chemical potential describing the superheating of one phase with respect to the other [18]. $\Delta\mu$ is proportional to the overvoltage applied to the junction, and the delay time is inversely proportional to the rate of critical nucleation and follows the form $t_d \sim Ae^{B/(V-V_R)}$ [18].

One complication in understanding the transport mechanism is the fact that in Fe_3O_4 there is a significant amount of electronic short-range order (SRO) above T_v [114]. Therefore, the traditional one-particle concepts do not apply. For instance, the increase in DC conductivity with temperature above T_v does not preclude describing it in terms of band conduction, since the breakdown of SRO with temperature leads to a thermally activated band conductivity [114]. However, since hopping models also yield a thermally activated DC conductivity, it is often difficult to separate DC band conduction from hopping conduction mechanisms.

Many studies have noted the occurrence of two types of strong interaction between the valence electrons in Fe_3O_4: the electron-phonon interaction resulting in the formation of small polarons and the intersite Coulomb interaction that leads to a strong correlation or high SRO [115-116]. Thus, in a theory of small polaron conductivity, the polaronic SRO due to intersite SP-SP interaction has to be taken into account. It appears that the main DC conductivity mechanism below T_v and slightly above T_v is band conduction of strongly correlated SP. At higher temperatures, a gradual transition from SP band conduction to SP hopping conduction should occur. DC conductivity of Fe_3O_4 can be explained by combining both conduction models.

The small polaron, formed by the extra spin-down B-site electron at the Fe^{2+} ions, can be expressed by the following Hamiltonian [117]:

$$H=H_0+H_1 \tag{5}$$

$$H_1= -t\Sigma_{<ij>} \Psi_{ij} \mathbf{c}_i^{+}\mathbf{c}_j \tag{6}$$

$$H_0= -E_b\Sigma_i \mathbf{n}_i + (1/2)\Sigma_{i\neq j} U_{ij} \mathbf{n}_i \mathbf{n}_j + \Sigma_{qv} \omega_{qv}\mathbf{b}_{qv}^{+}\mathbf{b}_{qv} \tag{7}$$

$$E_b=\Sigma_{qv}|A_{qv}|^2\omega_{qv}^{-1} \tag{8}$$

$$U_{ij}=V_{ij} - 2\Sigma_{qv}|A_{qv}|^2\omega_{qv}^{-1}\cos\{q(R_i-R_j)\} \tag{9}$$

$$\Psi_{ij}=\exp\{\Sigma_{qv}(\Delta_{qvij}\mathbf{b}_{qv}+ - \Delta_{qvij}^{*}\mathbf{b}_{qv})\} \quad (10)$$

$$\Delta_{qvij}=A_{qv}^{*}\omega_{qv}^{-1}(e^{-iqR}{}_{i} - e^{-iqR}{}_{j}) \quad (11)$$

where

i, j label the B sites

$\mathbf{n}_i=\mathbf{c}_i+\mathbf{c}_j$ and $\mathbf{c}_i+$, $\mathbf{b}_{qv}^{+}$ are the creation operators for a SP and a displaced phonon

t=nearest-neighbor transfer integral

E_b=SP binding energy in t=0 limit

A_{qv}=electron-phonon coupling

U_{ij}=effective SP-SP interaction energies

and V_{ij}=Coulomb integrals in the absence of phonons.

The model is considered in the narrow-band limit ($t<<E_b$), so the transfer term H_1 is treated in the lowest-order perturbation approach and is rewritten as

$$H_1=H_b+H_h \quad (12)$$

$$H_b= -\mathbf{t}\Sigma_{<ij>}\mathbf{c}_i+\mathbf{c}_j \quad (13)$$

$$\mathbf{t}=te^{-S}{}_{T} \quad (14)$$

$$S_T=S_0\coth(\beta\omega_0/2) \quad (15)$$

H_b describes SP transitions without changes of the phonon occupation numbers (diagonal transitions) and results in an effective SP band. H_h describes transitions that are accompanied by multi-phonon processes (non-diagonal transitions). The nearest-neighbor SP-SP interactions U_1 and S_0 are related by

$$U_1=(4.84/\varepsilon_x - 0.47S_0)\ \text{eV} \quad (16)$$

where ε_x is the high-frequency background dielectric constant [115]. Because of the spinel structure of Fe_3O_4, the interaction U_1 mostly determines the SRO properties of the B site lattice, while the LRO is stabilized by a different interaction an order of magnitude smaller than U_1 [118]. The relevant characteristics of the physical quantities and mechanisms mentioned here are determined by the degree of SRO. From experiments, the relation $U_1 >> kT_v > \mathbf{t}$ is assumed. This gives a near-perfect SRO up to T_v.

The first-order character of the Verwey transition is a SRO effect. If the free energies of the LRO phase and the phase without LRO are compared as functions of temperature, then according to the Anderson property and the macroscopic ground-state degeneracy of the SRO states, the entropy in the phase without LRO has a significant value at T_v, generating a very steep slope of the free energy. In the LRO phase (i.e. without any ground-state degeneracy), the entropy has a very small value up to T_v. Therefore, the two free energy curves intersect at T_v, indicating a first-order Verwey transition. In the Hartree approximation, which ignores SRO, the transition is found to be second-order. This underscores the fact that the first-order nature of the Verwey transition is a SRO effect.

Below T_v the LRO has roughly the same degree as at T=0; at T_v it suddenly vanishes. Since the SRO below T_v is enhanced by LRO, it drops abruptly at T_v but is large just above T_v. As the temperature increases, the SRO breaks down. Heat capacity measurements give an entropy change at T_v of $\Delta S_v \sim 6$ J/mol-K [119-120]. If ΔS_v is compared with the configurational entropy for complete charge disorder, $S_{max}=2R\ln 2=11.5$ J/mol-K, and the very low value of $S(T_v^-)$ is taken into consideration, the sharp deviation of the entropy from S_{max} above T_v illustrates the high degree of SRO above the Verwey transition.

Below T_v, there are two sub-bands, with a width of approximately $6\mathbf{t}$, separated by a gap of $E_g \sim 2U_1$. At T=0 the band at $2U_1$ is fully occupied while the $4U_1$ band is empty. At T_v the sudden drop in SRO causes the advent of another sub-band at the chemical potential $\mu(T) \sim 3U_1$. In accordance with the breakdown in SRO with increasing temperature, the density of states in the sub-bands at μ and $\mu \pm U_1$, respectively, increases and decreases with temperature. The sub-band at $2U_1$ and the band at $4U_1$ are denoted by

the SP valence and SP conduction band, respectively. Because $kT<<U_1$, the density of n-type current carriers, n_n, thermally activated across the gap $E_g \sim 2U_1$ is very small, and the system of those carriers can be thought of as a dilute gas of weakly interacting quasi-particles. Their contribution to the band conduction stems from the motion in the SP conduction band, meaning that an n-type quasi-particle moves between sites that are surrounded by four SP. This site environment is created by the nearly perfect SRO and provides a rigid background over which the quasi-particles move. Meanwhile, the thermal activation causes a small density n_p for p-type quasi-particles in the SP valence band, where $n_p=n_n$. Figure 2.5 gives a qualitative representation.

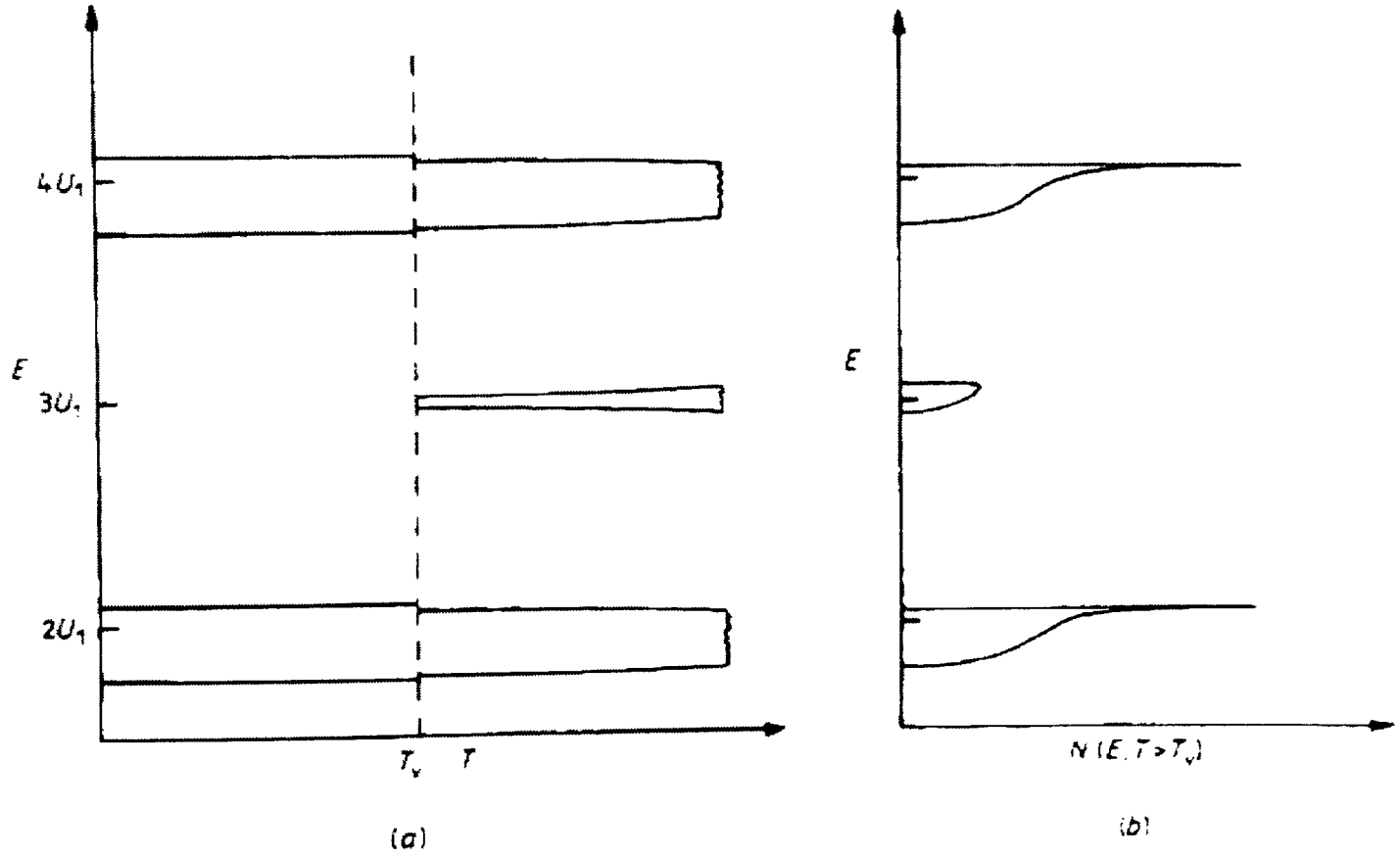

Figure 2.5. Energy level diagrams for magnetite. a) shows the band scheme and b) shows the one-particle density of states (for constant $T>T_V$). [121]

In addition to the excitation of single n- and p-type current carriers, thermal excitation of n-p nearest neighbor pairs also occurs in magnetite. The creation of these pairs manifests in the charge transfer to an empty nearest-neighbor site. Since there is almost perfect SRO below T_v, this process requires the energy U_1, as does the dissociation of the n-p pairs into single current carriers; this is due to the almost perfect SRO in the B-site lattice [114]. Therefore, the excitation of current carriers by the formation of n-p pairs requires the same energy ($2U_1$) as the direct activation of single particles and holes, and the DC band conductivity below the Verwey transition follows the Arrhenius law with the activation energy $E_a=U_1$.

For the DC band conductivity above T_v, the conduction inside the band at μ is metal-like. However, the destruction of SRO with increasing temperature gives a thermally activated concentration of current carriers and an increasing density of states in this band. Above the Verwey transition the quasi-particle concept and the semiconductor-like model that are valid for $T<T_v$ break down. The sharp decrease in SRO at T_v results in a discontinuous increase in the DC conductivity at T_v, while the destruction of SRO with increasing temperature gives a thermally activated DC conductivity.

The SP band conductivity for $\omega<<U_1$ obeys the Drude law

$$\sigma_b^{v}(\omega)=\sigma_b^{v}/(1+\omega^2\tau^2) \tag{17}$$

where τ is the mean transport relaxation time. The temperature dependence of τ is assumed to be negligible in the temperature region where the band conduction is essential ($T<400$ K).

Below the Verwey transition, the DC conductivity obeys the Arrhenius law

$$\sigma_b^{v}(T<T_v)=\sigma_0^{v}\beta U_1 e^{-\beta U_1} \tag{18}$$

with the prefactor σ_0^{v} showing only a weak temperature dependence.

With increasing temperature, the SP hopping conductivity adds to the total conductivity, since the rise in the mean phonon occupation number increases the probability of multi-phonon processes.

For the SP hopping conduction in the presence of SRO in the high-temperature region $T>T_0(>T_v)$, we have

$$kT_0=\omega_0\{2\ln[2S_0+(1+4S_0^2)^{1/2}]\}^{-1} \quad (19)$$

The hopping conduction for $T_0<T<500$ K stems from non-adiabatic SP hopping in the quantal (sub-barrier tunneling) regime.

Resistance switching in magnetite can be explained in terms of a self-heating model caused by Joule heating. At high enough power inputs, a threshold is passed and the sample develops negative resistance according to the equation

$$-\mathbf{J}\cdot\mathbf{E} = -\rho C_p(\delta T/\delta t) + \nabla\cdot(\kappa\nabla T) \quad (20)$$

where **J** is the current density and **E** is the electric field [122].

3. EXPERIMENTAL

3.1. METHODS

As discussed in the prior literature review, resistance switching behavior has been observed in many transition metal oxides, including magnetite thin films deposited via methods such as magnetron sputtering and molecular-beam epitaxy. While the underlying theory is the same regardless of deposition method, the practical implementation of the resistance switching phenomenon calls for a simpler fabrication method. The purpose of this thesis is to show that resistance switching also occurs in magnetite films fabricated via electrodeposition, a novel production method that shows promise for use in the computer memory industry.

The magnetite thin films examined here deposit via a two-step electrochemical/chemical (EC) mechanism, and the surface concentrations of Fe(III) and Fe(II) can be tightly controlled by varying the applied potential. The stock solution used had 90 mM Fe(III), 100 mM triethanolamine (TEA), and 2M NaOH and was stirred at 200 rpm and 80 °C. The solution was prepared by slowly adding Fe(III) dissolved in water to a stirred solution of NaOH and TEA. The $Fe_2(SO_4)_3$ hydrate, TEA and NaOH were purchased from Aldrich (Milwaukee, WI). The solution slowly decomposed in air over a period of several days. For the resistance switching measurements, the films were deposited onto glass microscope slides covered with a 1000-Å layer of Au(111). In order to measure the lattice parameter along the *a*-axis, the films were deposited onto stainless steel pucks. Since both of the substrates and magnetite exhibit fcc crystal structures with lattice parameters which are multiples of each other's, the lattice matching is good and the property measurements are comparable between substrates [123]. The deposition of Fe_3O_4 is thought to obey the following equations [124]:

$$Fe(TEA)^{3+} + e^- \rightarrow Fe^{2+} + TEA \tag{21}$$

$$Fe^{2+} + 2Fe(TEA)^{3+} + 8OH^- \rightarrow Fe_3O_4 + 2TEA + 4H_2O \tag{22}$$

The electrochemical experiments were done using an EG&G Princeton Applied Research model 2273 (Oak Ridge, TN) potentiostat/galvanostat. The depositions were performed in an undivided cell with the solution exposed to the atmosphere. The reference electrode was Ag/AgCl. The cyclic voltammogram was run on a 0.02 cm^2 Au electrode in an unstirred solution at 50 mV/s. The linear sweep voltammogram was run at the same scan rate but in a stirred solution on a Au(111) single crystal.

The XRD scans were done on a high-resolution Philips X'Pert MRD diffractometer (Eindhoven, The Netherlands). The primary optic module was a combination Göbel mirror and 2-crystal Ge(220) 2-bounce hybrid monochromator; the secondary optics module was a 0.18° parallel plate collimator. The hybrid monochromator produces pure Cu $K_{\alpha 1}$ radiation (λ=0.154056 nm) with a divergence of 25 arc seconds. Asymmetric 2Θ scans were used to confirm that the thin films were indeed magnetite, and Rietveld analysis was employed to obtain the lattice parameters along the crystallographic *a*-axis.

The morphology of the films was examined using a Hitachi S4700 SEM (Pleasanton, CA). To capture a cross-sectional image, the microscope slide was cleaved and viewed edge-on.

To examine the resistance switching characteristics, the sample was maintained at a temperature (here 77 K) below T_v (120 K) at which the material is still insulating and in a correlated ordered state. When either the applied current or voltage is swept, magnetite experiences an insulator-to-metal phase transition and the resistance sharply decreases. High-to-low resistance switching in single-crystal magnetite has been credited to either an insulator-to-metal phase transition driven by Joule heating caused by current flow through the sample or to an electric-field driven transition due to strong electron-phonon coupling.

For this study, pressed In contacts were made to the film and to the Au(111) substrate. This arrangement ensures perpendicular transport of charge through the sample. The sample was held below the Verwey transition via immersion in liquid nitrogen at 77 K, and the bias was measured as the applied current was swept from 0 to 2

A at a scan rate of 50 mA/s. Multiple films deposited at biases of -1.01 V and -1.065 V vs. Ag/AgCl, respectively, were examined.

3.2. RESULTS AND DISCUSSION

The asymmetric XRD 2Θ scans seen in Figure 3.1 show that crystalline magnetite (Fe_3O_4) is being deposited onto the substrates, with strong peaks from the (311) and (440) reflections. The electrodeposited film is not maghemite, as indicated by the absence of the mixed-index reflections characteristic of γ-Fe_2O_3. For thin films, asymmetric scans are preferred because the films are textured, making accurate phase identification difficult. An asymmetric scan holds the incident angle constant while the angle between the sample and detector is allowed to vary. This method largely avoids detecting the planes perpendicular to the surface normal. However, symmetric scans are better suited for determining preferred orientations.

a)

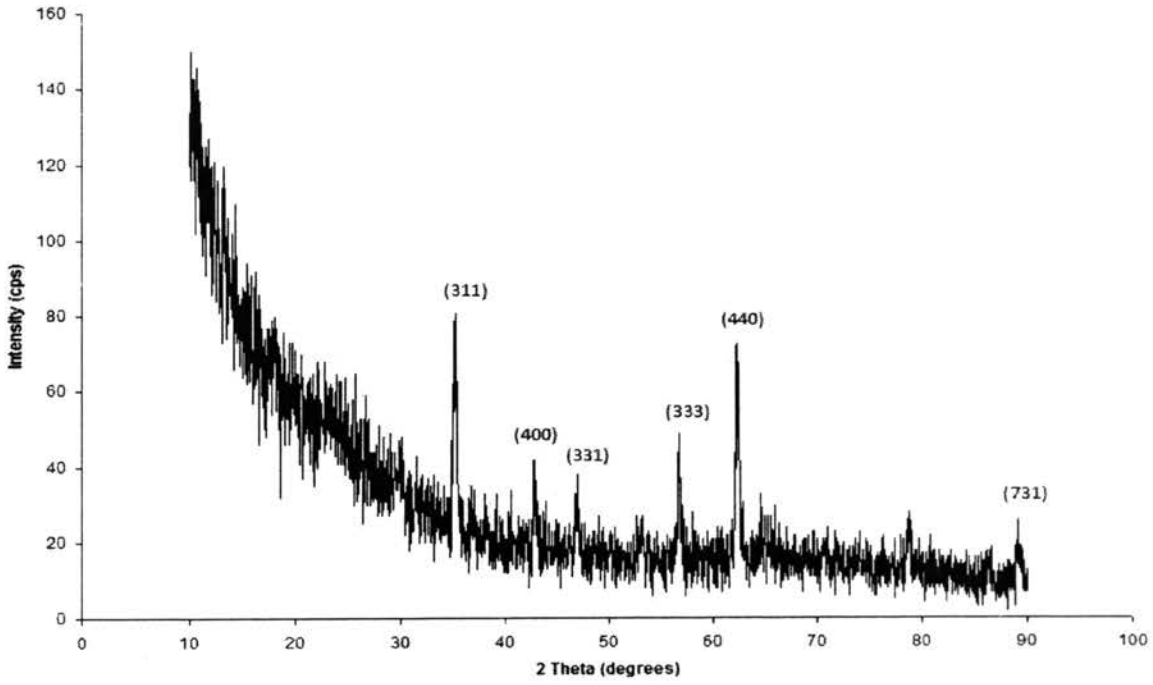

b)

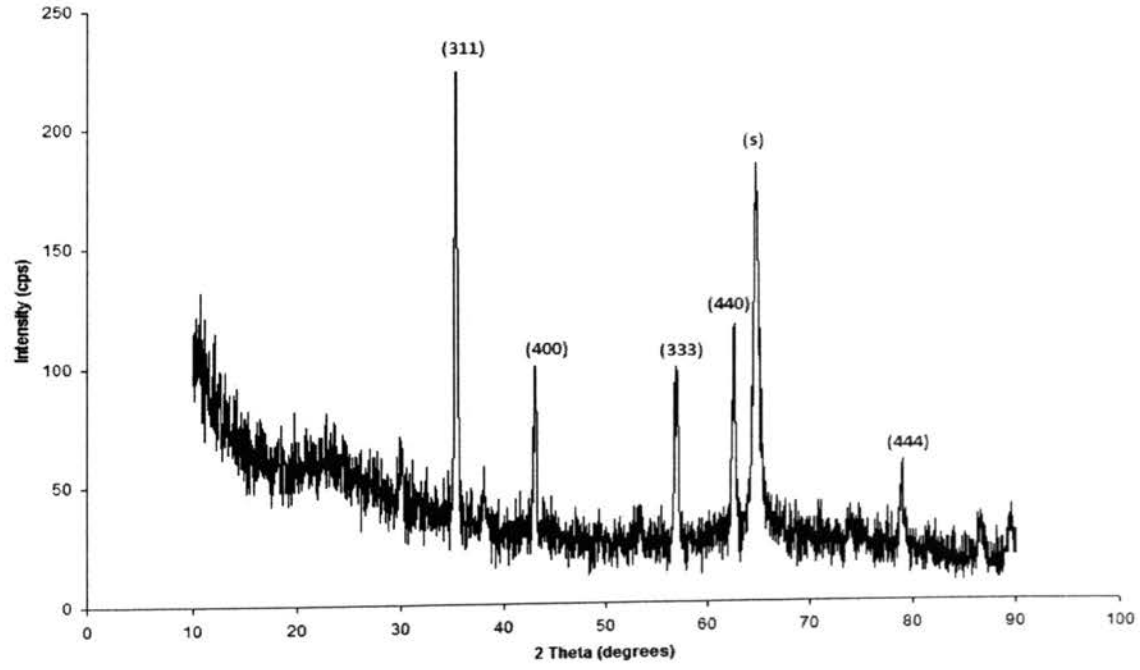

Figure 3.1. Asymmetric XRD 2Θ scans of films. a) was deposited at -1.01 V and b) at -1.065 V. (s) denotes a substrate peak.

The surface morphology of the films can be seen in the SEM micrographs presented in Figure 3.2. A film deposited at a) -1.01 V vs. Ag/AgCl shows an ordered,

triangular morphology, while the -1.065 V film shown in plan-view in b) evidences a globular morphology. The columnar nature of the morphology can clearly be seen in the cross-sectional micrograph c).

a)

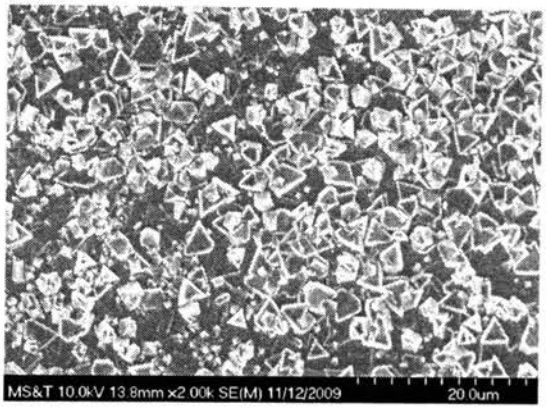

b)

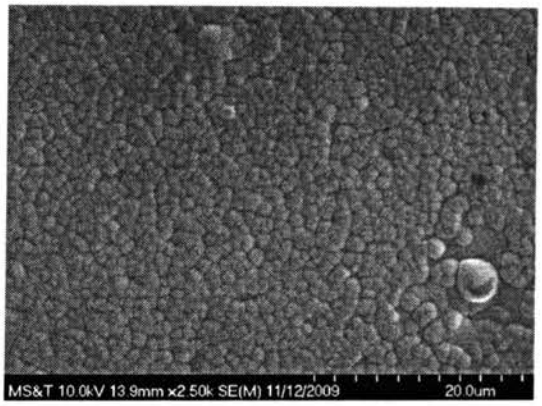

c)

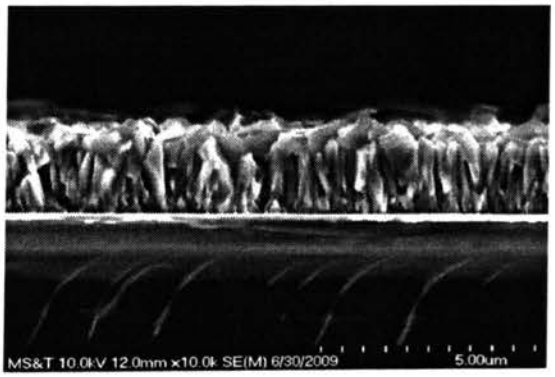

Figure 3.2. SEM micrographs of films. a) shows a film grown at -1.01 V, b) at -1.065 V, and c) at -1.065 V in cross-section.

At 80 °C, the anodic and cathodic peaks are separated by 100 mV, as is evident from the cyclic voltammogram of the unstirred stock solution shown in Figure 3.3. Reduction begins around -1.00 V and reaches a cathodic peak at -1.13 vs. Ag/AgCl, while the anodic peak is found at -1.03 V. Fe_3O_4 starts to deposit at a potential of -0.99 V vs. Ag/AgCl; the reaction becomes mass-transport limited at -1.2 V, as seen in the linear sweep voltammogram of the stirred stock solution in Figure 3.4 [124]. The mass transport is mainly controlled by convection [124].

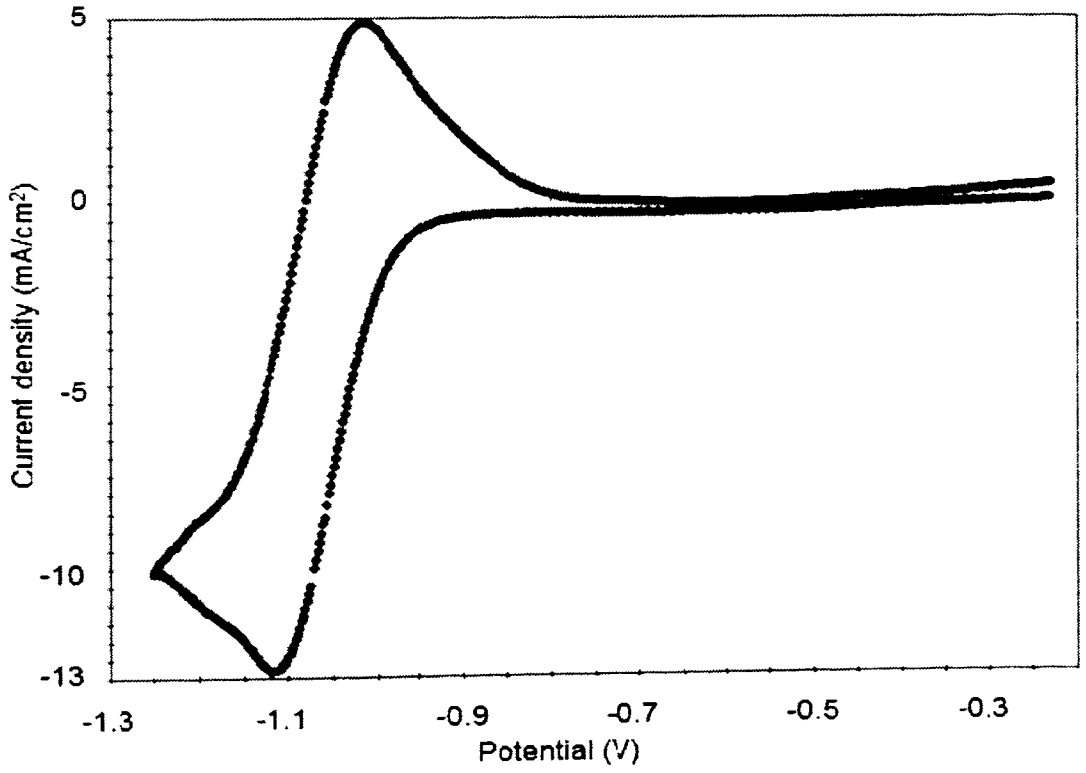

Figure 3.3. Cyclic voltammogram of unstirred stock solution.

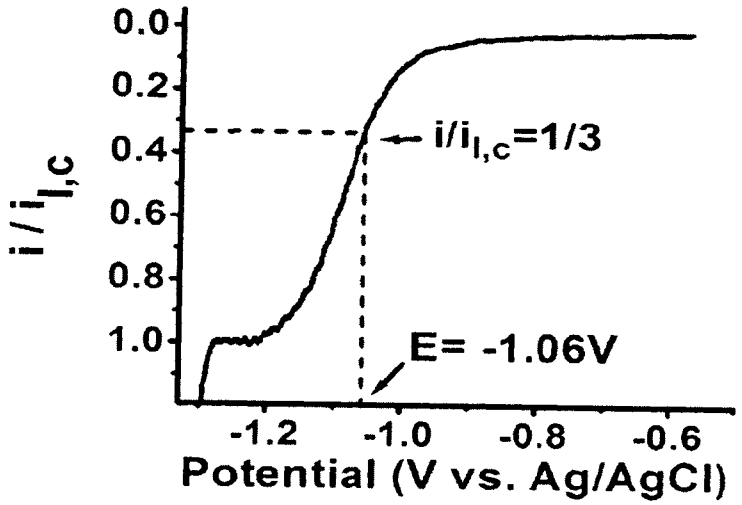

Figure 3.4. Linear sweep voltammogram of stirred stock solution.

At low overpotentials where I=0, the surface concentration of $Fe(TEA)^{3+}$ should approach zero. The surface concentration can be calculated from [124]

$$I/I_{l,c} = [C_{Fe(III)}(bulk) - C_{Fe(III)}(surface)]/C_{Fe(III)}(bulk) \quad (23)$$

where I is the measured current, $C_{Fe(III)}(bulk)$ is the bulk concentration of Fe(III) in solution, and $C_{Fe(III)}(surface)$ is the Fe(III) concentration at the electrode surface. Stoichiometric Fe_3O_4 should deposit at -1.06 V vs. Ag/AgCl, where $I/I_{l,c}=1/3$. At potentials more positive than -1.06 V, the film should have an excess of Fe(III); at potentials more negative than -1.06 V, there should be an excess of Fe(II).

Fe_3O_4 deposited at -1.05 to -1.06 V vs. Ag/AgCl has an *a*-axis lattice parameter that agrees well with the accepted value for Fe_3O_4. In addition, the temperature of the Verwey transition reaches a maximum of 123 K for a film deposited at -1.065 V, compared to 103 K for a film deposited at -1.01 V [124]. Since non-stoichiometry has been shown to lower the temperature at which the Verwey transition occurs, these results suggest that nearly stoichiometric magnetite is produced at -1.065 V vs. Ag/AgCl. This

is supported by the graph of lattice parameters along the *a*-axis over a range of potentials in Figure 3.5, which shows the variation in stoichiometry for films deposited onto stainless steel substrates. The dashed line represents the stoichiometric lattice parameter for magnetite. The data are reproducible, with an uncertainty of ±0.005 nm. While Fe^{3+} is a smaller ion than Fe^{2+}, the films with excess Fe^{3+} ions exhibit a larger lattice parameter than those without. This may be due to the creation of oxygen vacancies in the films deposited at more positive potentials, which are thicker than films grown at more negative potentials. This results in a higher charge density and more current being passed through the sample, which produces Joule heating. At higher temperatures, more vacancies are formed [125].

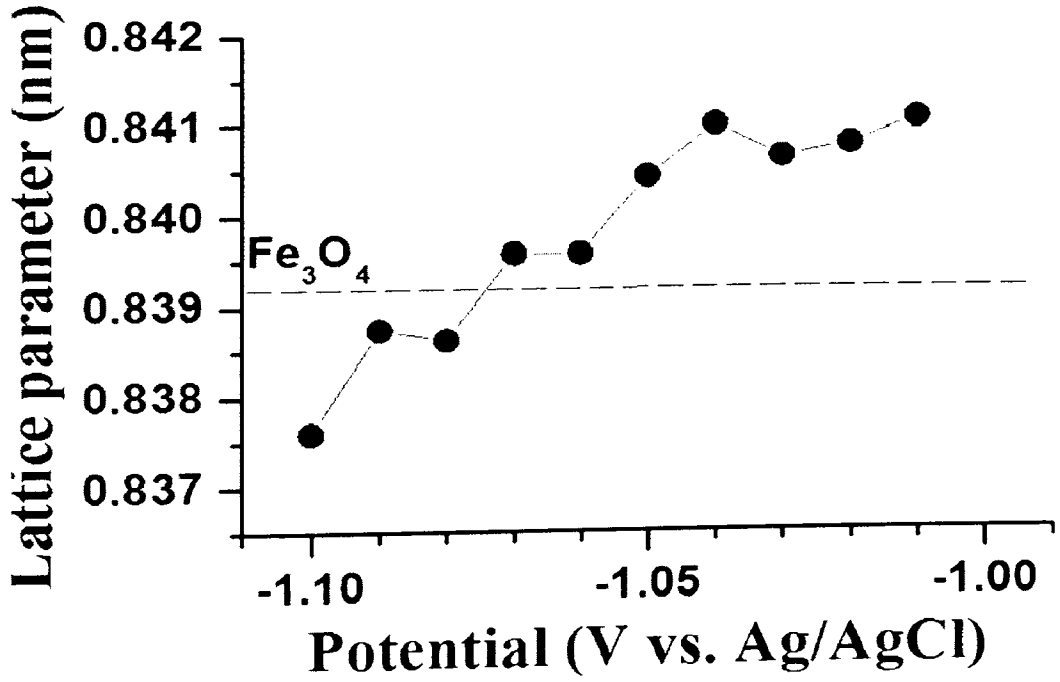

Figure 3.5. Lattice parameters along the *a*-axis over a range of potentials.

When the resistance switching behavior of the films is examined, it is evident that electrodeposited magnetite thin films do show an insulator-to-metal transition. The curve for a -1.065 V film is non-Ohmic, but it displays abrupt low-to-high resistance switching at applied biases of +0.95 and -0.93 V vs. Ag/AgCl, as seen in Figure 3.6. While this effect is obvious for films deposited on Au-on-glass substrates, it has not been observed in films grown on Au(111) single-crystal substrates. For that case, only magnetite superlattices (crystallographically coherent multilayers) show resistance switching behavior [124].

Unlike the high-to-low resistance switching observed at higher biases, the low-to-high resistance switching seen here is not caused by the insulator-to-metal phase transition that occurs at T_v, since a similar transition has been seen in nanophase Fe_3O_4 at room temperature [126]. Odagawa credited this behavior to field-driven oxidation of Fe_3O_4 to the less conductive γ-Fe_2O_3 (maghemite; a=0.83515 nm, space group $P4_132$) at the interface between the metallic anode electrode and the Fe_3O_4 film [127]. That study found maghemite at the interface using Raman spectroscopy. While further study is required for verification, it is assumed that is also the case here.

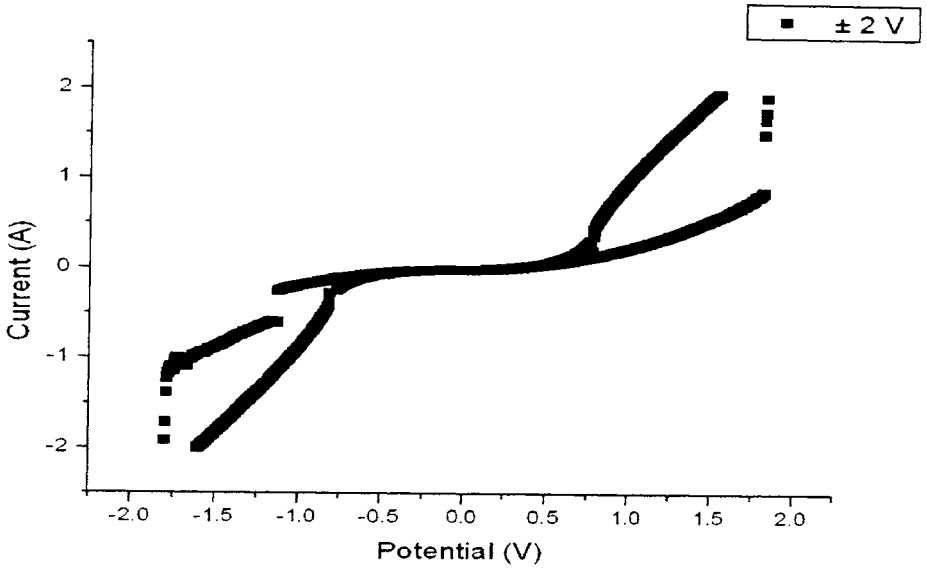

Figure 3.6. IV curve for -1.065 V film with a charge density of 1 C/cm^2.

It can also be seen in Figure 3.7 that films grown at higher and lower charge densities, and therefore larger and smaller thicknesses, still show resistance switching behavior. This tolerance for changes in the deposition conditions would be useful in an industrial setting, where such parameters can be difficult to tightly control. Furthermore, these results support the scalability of magnetite RRAM, since the thinner films still perform.

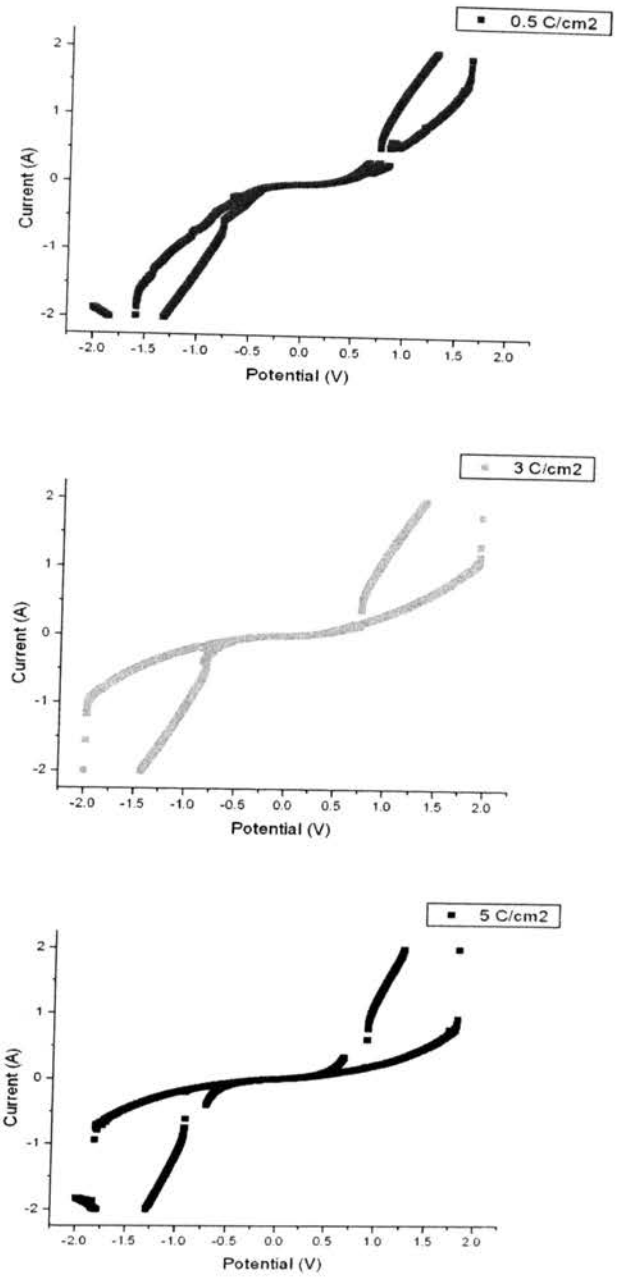

Figure 3.7. IV curves for films with charge densities of a) 0.5, b) 3 and c) 5 C/cm^2.

In terms of a proposed resistance switching mechanism, the presence of maghemite is consistent with the increased resistance seen at the anode, since it has a high resistivity of above 10^2 Ω-cm [128]. This suggests that the bistable change occurs in the nanometer-scale region and is consistent with the oft-proposed model in which

switching is initiated at a local region near an interface between an oxide and a metal [129-135]. The resistance switching behavior can be expressed in terms of the redox reaction [136]

$$2Fe_3O_4 + O^{2-} \leftrightarrow 3\gamma - Fe_2O_3 + 2e^- \quad (24)$$

which occurs near the anode interface when an electric field is applied. The electroformed higher resistance is caused by the migration of O^{2-} ions in the Fe_3O_4 film. The electron extraction from an anode induced by the application of negative voltage pulses would result in O^{2-} migration and accumulation around the anode, creating a γ-Fe_2O_3 layer that covers the anode. The O^{2-} used in the reaction may have been preexisting in the anode, which is corroborated by results showing electroforming and stable switching behaviors even in vacuum [136]. Likewise, appropriate amounts of O^{2-} in the Fe_3O_4 layer are vital for reliability, such as the retention time and endurance of the device [137-138]. The low resistance state is caused by reduction of the maghemite layer on the anode. Electron injection from the anode upon the application of positive voltage pulses drives the migration of O^{2-} ions and produces a local spot of Fe_3O_4 in the maghemite layer on the anode. Afterwards, bistable switching is caused by a reversible redox reaction at the local spot in the same manner. This is also supported by the recently put-forth mechanism in which the local change in oxygen concentration at the anode interface is essential to obtaining a secure switching response [139].

4. CONCLUSIONS

Magnetite thin films were electrodeposited onto 1000-Å Au-on-glass and stainless steel substrates via reduction of a Fe(III)-triethanolamine complex in aqueous alkaline solution at biases of -1.01 V and -1.065 V vs. Ag/AgCl. The films were characterized using electrochemical methods, including cyclic voltammetry and linear sweep voltammetry, as well as X-ray diffraction and scanning electron microscopy. Pressed In contacts were made to the film and to the gold substrate, and when the films were held below the Verwey transition temperature of 120 K, they clearly displayed bipolar resistance switching behavior as the applied current or voltage was swept. Since the previous literature on resistance switching has dealt with either the phenomenon in other materials or in forms of magnetite other than electrodeposited thin films, this is a significant result. While verification with Raman spectroscopy is still required, the resistance switching behavior is likely caused by the migration of O^{2-} ions in the film and a reversible redox reaction that occurs at the anode. These results demonstrate that electrodeposition can produce viable, scalable magnetite thin films for resistance switching applications, and that the method described here can be employed for use in the non-volatile computer memory industry. Future work remains to be done on the statistical reliability of these electrodeposited thin films as well as on their use in the form of superlattices.

BIBLIOGRAPHY

[1] G.I. Meijer, *Science* **2008**, *319*, 1625-1626.

[2] http://www.itrs.net/reports.html. International Technology Roadmap for Semiconductors (ITRS 2006).

[3] Y. Dong, G. Yu, M.C. McAlpine, W. Lu and C.M. Leiber, *Nano Letters* **2008**, *8*, 386-391.

[4] A. Beck, J.G. Bednorz, Charles Gerber, C. Rossel and D. Widmer, *Applied Physics Letters* **2000**, *77*, 139-141.

[5] M.J. Lee, Y. Park and D.S. Suh, *Advanced Materials* **2007**, *19*, 3919-3923.

[6] R. Waser and M. Aono, *Nature Materials* **2007**, *6*, 833-840.

[7] B.J. Choi, D.S. Jeong and S.K. Kim, *Journal of Applied Physics* **2005**, *98*, 033715.

[8] J.E. Brewer, V.V. Zhimov and J.A. Hutchby, *J.A. IEEE Circuits Devices Magazine* **2005**, *21*, 13-20.

[9] G. Muller, T. Happ and M. Kund, *IEDM Technical Digest* **2004**, 567-570.

[10] R.A. de Groot, *Phys. Rev. Letters* **1983**, *50*, 2024.

[11] S.A. Wolf and D. Treger, *IEEE Trans. Magn.* **2000**, *36*, 2748.

[12] Z. Kakol and J.M. Honig, *Phys. Rev. B* **1989**, *40*, 9090.

[13] Z. Zhang and S. Satpathy, *Phys. Rev. B* **1991**, *44*, 13319.

[14] V.I. Anisimov, I.S. Elfimov, N. Hamada and K. Terakura, *Phys. Rev. B* **1996**, *54*, 4387.

[15] Y.S. Dedkov, U. Rudiger and G. Guntherodi, *Phys. Rev. B* **2002**, *65*, 064417.

[16] T.A. Sorenson, S.A. Morton, D.G. Waddill and J.A. Switzer, *J. Am. Chem. Soc.* **2002**, *124*, 7604.

[17] G. Hu and Y. Suzuki, *Phys. Rev. Letters* **2002**, *89*, 276601.

[18] R. C. Morris, J.E. Christopher and R.V. Coleman, *Phys. Rev.* **1969**, *184*, 565-573.

[19] E.J. Verwey and P.W. Haayman, *Physica* **1941**, *8*, 979.

[20] T.W. Hickmott, *J. Appl. Physics* **1962**, *33*, 2669-2682.

[21] G. Dearnaley, A.M. Stoneham and D.V. Morgan, *Rep. Prog. Phys.* **1970**, *33*, 1129-1191.

[22] D.P. Oxley, *Electrocomponent Science & Technology UK* **1977**, *3*, 217-224.

[23] H. Pagnia and N. Sotnik, *Phys. Status Solidi* **1988**, *108*, 11-65.

[24] A. Asamitsu, Y. Tomioka, H. Kuwahara and Y. Tokura, *Nature* **1997**, *388*, 50-52.

[25] M.N. Kozicki, M. Yun, L. Hilt and A. Singh, "Applications of programmable resistance changes in metal-doped chalcogenides," *Pennington NJ USA: Electrochemical Society* 1999, 298-309.

[26] A. Beck, J.G. Bednora, C. Gerber, C. Rossel and D. Widmer, *Appl. Phys. Lett.* **2000**, *77*, 139-141.

[27] A. Asamitsu, Y. Tomioka, H. Kuwahara and Y. Tokura, *Nature* **1997**, *388*, 50-52.

[28] A. Sawa, T. Fujii, M. Kawasaki and Y. Tokura, *Appl. Phys. Lett.* **2004**, *85*, 4073-4075.

[29] S. Lee, A. Fursina and J.T. Mayo. *Nature Materials* **2007**, *6*, 833-840.

[30] W.W. Zhuang, W. Pan, B.D. Ulrich, J.J. Lee and L. Stecker. *Tech. Dig. IEDM* **2002**, 193.

[31] C. Yoshida, K. Tsunoda and H. Noshiro, *Appl. Phys. Lett.* **2007**, *91*, 223510.

[32] R. Waser and M. Aono, *Nature Materials* **2007**, *6*, 833-840.

[33] D.S. Jeong, H. Schroeder and R. Waser, *Electrochemical Solid State Letters* **2007**, *10*, G51-53.

[34] J.G. Simmons and R.R. Verderber, *Proc. R. Soc. Lond. A* **1967**, *301*, 77-102.

[35] A. Sawa, T. Fujii, M. Kawasaki and Y. Tokura, *Appl. Phys. Lett.* **2006**, *88*, 232112.

[36] T. Fujii, M. Kawasaki, A. Sawa, H. Akoh, Y. Kawazoe and Y. Tokura. *Appl. Phys. Lett.* **2005**, *86*, 012107.

[37] D. Lee, I.H. Doh, J. Choi and S.H. Noh, *Proc. Non-Volatile Memory Technology Symposium* **2006**, 89-93.

[38] M.J. Rosenberg, I.H. Inoue and M.J. Sanchez, *Appl. Phys. Lett.* **2006**, *88*, 033510.

[39] L. Esaki, R.B. Laibowitz and P.J. Stiles, *IBM Tech. Discl. Bull.* **1971**, *13*, 2161.

[40] M. Faraday, *Philosophical Transactions of the Royal Society of London* **1833**, *123*, 507-522.

[41] H. Kohlstedt, N.A. Pertsev, J.R. Contreras and R. Waser, *Phys. Rev. B* **2005**, *72*, 125341.

[42] M.N. Kozicki, M. Yun, L. Hilt and A. Singh, *Pennington NJ USA: Electrochemical Society* **1999**, 298-309.

[43] T. Baiatu, R. Waser and K.H. Hardtl, *J. Am. Ceram. Soc.* **1990**, *73*, 1663-1673.

[44] Y. Tokura and N. Nagaosa, *Science* **2000**, *288*, 462.

[45] M. Imada, A. Fujimon and Y. Tokura, *Rev. Mod. Phys.* **2004**, *76*, 323.

[46] M. Ziebe, *Rep. Prog. Phys.* **2002**, 65, 143.

[47] I. Zunc, J. Fabian and S.D. Sarma, *Rev. Mod. Phys.* **2004**, *76*, 323.

[48] M. Fomm, Y.S. Dedkov, R. Pentcheva, U. Rudiger and G. Guntherodt, *J. Phys.: Condensed Matter* **2007**, *19*, 315217.

[49] P.J. Freud and A.Z. Hed, *Phys. Rev. Lett.* **1969**, *23*, 1440-1443.

[50] P.A. Miles, W.B. Westphal and A. von Hippel, *Rev. Mod. Phys.* **1957**, *29*, 279-307.

[51] N. Lenge, H. Kronmuller and F. Walz, *J. Phys. Soc. Japan* **1984**, *53*, 1406-1414.

[52] W. Haubenreisser, *Phys. Status Solidi b* **1961**, *1*, 619-635.

[53] A.A. Samokhvalov, N.M. Tutikov and G.P. Skornyakov, *Fiz. Tverd. Tela* **1968**, *10*, 2760-2764.

[54] D.L. Camphausen, *Solid State Communications* **1972**, *11*, 99-103.

[55] P. Muret, *Solid State Communications* **1974**, *14*, 1119-22.

[56] Z. Simsa, *Phys. Status Solidi b* **1979**, *96*, 581-587.

[57] A.A. Fursina, R.G.S. Sofin, I.V. Shvets and D. Natelson, *Phys. Rev. B* **2009**, *79*, 245131.

[58] S. Lee, A. Fursina, J.T. Mayo and C.T. Yavuz, *Nat. Mater.* **2008**, *7*, 130-133.

[59] D.J. Huang, H.J. Lin, J. Okamoto, K.S. Chao and H.T. Jeng, *Phys. Rev. Lett.* **2006**, *96*, 096401.

[60] N. Sugimoto, S. Onoda and N. Nagaosa, *Phys. Rev. B* **2008**, *78*, 155104.

[61] A. Sawa, *Materials Today* **2008**, *11*, 28-36.

[62] T.W. Hickmott, *J. Appl. Phys.* **1962**, *33*, 2269.

[63] K. Kinoshita, T. Tamura, M. Aoki, Y. Sugiyama and H. Tanaka, *Appl. Phys. Lett.* **2006**, *89*, 103509.

[64] K.M. Kim, B.J. Choi and C.S. Hwang, *Appl. Phys. Lett.* **2007**, *90*, 242906.

[65] Z. Szot, W. Speier, G. Bihlmayer and R. Waser, *Nature Materials* **2006**, *5*, 312.

[66] A. Baikalov, Y.Q. Wang, B. Shen, B. Lorenz and S. Tsui, *Appl. Phys. Lett.* **2003**, *83*, 957.

[67] S. Tsui, A. Baikalov, J. Cmaidalka, Y.Y. Sun and Y.Q. Wang, *Appl. Phys. Lett.* **2004**, *85*, 317.

[68] X. Chen, N.J. Wu, J. Strozier and A. Ignatiev, *Appl. Phys. Lett.* **2005**, *87*, 233506.

[69] D.J. Seong, M. Jo, D. Lee and H. Hwang, *Electrochemical Solid State Letters* **2007**, *10*, H168.

[70] Y.B. Nian, J. Strozier, N.J. Wu, X. Chen and A. Ignatiev, *Phys. Rev. Lett.* **2007**, *98*, 146403.

[71] S.H. Jeon, B.H. Park, J. Lee, B. Lee and S. Han, *Appl. Phys. Lett.* **2006**, *89*, 042904.

[72] A. Sawa, T. Fujii, M. Kawasaki and Y. Tokura, *Appl. Phys. Lett.* **2004**, *85*, 4073.

[73] T. Fujii, M. Kawasaki, A. Sawa, H. Akoh and Y. Kawazoe, *Appl. Phys. Lett.* **2005**, *86*, 012107.

[74] A. Sawa, T. Fujii, M. Kawasaki and Y. Tokura, *Japanese Journal of Applied Physics* **2005**, *44*, L1241.

[75] R. Fors, S.I. Khartsev and A.M. Grishin, *Phys. Rev. B* **2005**, *71*, 045305.

[76] M.J. Rosenberg, I.H. Inoue and M.J. Sanchez, *Phys. Rev. Lett.* **2004**, *92*, 178302.

[77] M.J. Rosenberg, I.H. Inoue and M.J. Sanchez, *Appl. Phys. Lett.* **2006**, *88*, 033510.

[78] T. Oka and N. Nagaosa, *Phys. Rev. Lett.* **2006**, *95*, 266403.

[79] A. Sawa, T. Fujii, M. Kawasaki and Y. Tokura, *Appl. Phys. Lett.* **2006**, *88*, 232112.

[80] T. Fujii, M. Kawasaki, A. Sawa, Y. Kawazoe and H. Akoh, *Phys. Rev. B* **2007**, *75*, 165101.

[81] A. Sawa, *Materials Today* **2008**, *11*, 28.

[82] A. Sawa, T. Fujii, M. Kawasaki and Y. Tokura, *Appl. Phys. Lett.* **2004**, *85*, 4073.

[83] K. Szot, W. Speier, G. Bihlmayer and R. Waser, *Nature Materials* **2006**, *5*, 312.

[84] N. Sugimoto, S. Onoda and N. Nagaosa, *Phys. Rev. B* **2008**, *78*, 155104.

[85] M. Hasan, R. Dong, D.S. Lee, D.J. Seong and H.J. Choi, *J. of Semiconductor Tech. Sci.* **2008**, *8*, 65-78.

[86] H. Sim, H. Choi, D. Lee, M. Chang and D. Choi, *Tech. Dig. IEDM* **2005**, 758.

[87] K. Tsunoda, K. Kinoshita, H. Noshiro, Y. Yamazaki and T. Iizuka, *Tech. Dig. IEDM* **2007**, 767.

[88] S. Muraoka, K. Osano, Y. Kanzawa, S. Mitani and S. Fujii, *Tech. Dig. IEDM* **2007**, 779.

[89] I.G. Baek, M.S. Lee, S. Seo, M.J. Lee and D.H. Seo, *Tech. Dig. IEDM* **2004**, 587.

[90] L.V. Gasparov, D.B. Tanner, D.B. Romero, H.D. Drew and H. Berger, *Phys. Rev. B* **2000**, *62*, 7939-7944.

[91] F. Walz, *J. Phys. Condensed Matter* **2002**, *14*, R285-R340.

[92] J. Garcia and G. Subias, *J. Phys. Condensed Matter* **2004**, *16*, R145-R178.

[93] G. Subias, J. Garcia, J. Blasco, M.G. Proietti and H. Renevier, *Phys. Rev. Lett.* **2004**, *93*, 156408.

[94] G.K. Rozenberg, M.P. Pasternak, W.M. Xu, Y. Amiel and M. Hanfland, *Phys. Rev. Lett.* **2006**, *96*, 156402.

[95] I. Leonov, A.N. Yaresko, V.N. Antonov and J.P. Attfield, *Phys. Rev. B* **2006**, *74*, 165117.

[96] H.P. Pinto and S.D. Elliot, *J. Phys. Condensed Matter* **2006**, *18*, 10427-10436.

[97] P. Piekarz, K. Parlinski and A. Oles, *Phys. Rev. Lett.* **2006**, *97*, 156402.

[98] J. Smit, *Physica* (Amsterdam) **1951**, *17*, 612.

[99] T.R. McGuire and R.I. Potter, *IEEE Trans. Magn.* **1975**, *11*, 1018.

[100] J.P. Jan, *Solid State Physics*, **1957**, *5*, 1.

[101] R. Ramos, S.K. Arora and I.V. Shvets, *Phys. Rev. B* **2008**, *78*, 214402.

[102] I. Pallecchi, L. Pellegrino, A. Caviglia, E. Bellingeri and G. Canu, *Phys. Rev. B* **2007**, *76*, 174401.

[103] V.S. Amaral, A.A.C.S. Lourenco, J.P. Araujo, A.M. Pereira and J.B. Sousa, *J. Appl. Phys.* **2000**, *87*, 5570.

[104] M. Virer, *European Physics Journal B* **2006**, *51*, 1.

[105] M. Bibes, V. Laukhin, S. Valencia, B. Martinez and J. Fontcuberta, *J. Phys.: Condensed Matter* **2005**, *17*, 2733.

[106] S.K. Arora, R.G.S. Sofin, A. Nolan and I.V. Shvets, *J. Magn. Magn. Matter* **1997**, *176*, 111.

[107] D. Ihle and B. Lorenz, *J. Phys. C* **1986**, *19*, 5239.

[108] P. Piekarz, K. Parlinski and A.M. Oles, *Phys. Rev. Lett.* **2006**, *97*, 156402.

[109] P. Piekarz, K. Parlinski and A.M. Oles, *Phys. Rev. B* **2007**, *76*, 165124.

[110] S.M. Shapiro, M. Iizumi and G. Shirane, *Phys. Rev. B* **1976**, *14*, 200.

[111] Y. Yamada, N. Wakabayashi and R.M. Nicklow, *Phys. Rev. B* **1980**, *21*, 4642.

[112] I.V. Shvets, G. Mariotto, K. Jordan, N. Berdunov and R. Kantor, *Phys. Rev. B* **2004**, *70*, 155406.

[113] S.C. Abrahams and B.A. Calhoun, *Acta Cryst.* **1953**, *6*, 105.

[114] D. Ihle and B. Lorenz, *Phil. Mag. B* **1980**, *42*, 337-347.

[115] N.F. Mott, *Festkorperprobleme* **1979**, *19*, 331-361.

[116] D. Ihle, *Phys. Status Solidi b* **1984**, *121*, 217-224.

[117] D. Ihle, *Z. Phys. B* **1985**, *58*, 91-98.

[118] P.W. Anderson, *Phys. Rev.* **1956**, *102*, 1008-1013.

[119] E. Gmelin, N. Lenge and H. Kronmuller, *Phys. Status Solidi a* **1983**, *79*, 465-475.

[120] J.P. Shepherd, J.W. Koenitzer, R. Aragon, C.J. Sandberg and J.M. Honig, *Phys. Rev. B* **1985**, *31*, 1107-1113.

[121] D. Ihle and B. Lorenz, *J. Phys. C: Solid State Physics* **1986**, *19*, 5239-5251.

[122] T. Burch, P.P. Craig, C. Hedrick, T.A. Kitchens and J.I. Budnick, *Phys. Rev. Lett.* **1969**, *23*, 1444-1447.

[123] S. Mathur, S. Barth, U. Werner, F. Hernandez-Ramirez, and A. Romano-Rodriguez, *Advanced Materials* **2008**, *20*, 1550-1554.

[124] J. A. Switzer, R.V. Gudavarthy, E.A. Kulp, G. Mu, Z. He and A.J. Wessel, *J. Am. Chem. Soc.* **2010**, *152*, 1258-1260.

[125] D.R. Askeland and P.P. Phulé, *Essentials of Materials Science and Engineering*, Thomson, p. 120, **2004**.

[126] T.H. Kim, E.Y. Jang, N.J. Lee, D.J. Choi and K.J. Lee, *J. Nano Lett.* **2009**, *9*, 2229-2233.

[127] A. Odagawa, Y. Katoh, Y. Kanazawa, Z. Wei and T. Mikawa, *Appl. Phys. Lett.* **2007**, *91*, 133503.

[128] M. Naoe, Y. Hoshi and S. Yamanaka, *J. Appl. Phys.* **1982**, *53*, 2748.

[129] C. Rossel, G.I. Meijer, D. Bremaud and D. Widmer, *J. Appl. Phys.* **2001**, *90*, 2892.

[130] A. Baikalov, Y.Q. Wang, B. Shen, B. Lorenz and S. Tsui, *Appl. Phys. Lett.* **2003**, *83*, 957.

[131] I.H. Inoue, S. Yasuda, H. Akinaga and H. Takagi. e-print arXiv:cond-mat/0702564v1.

[132] K. Szot, W. Speier, G. Bihlmayer and R. Waser, *Nature Materials* **2006**, *5*, 312.

[133] B.J. Choi, D.S. Jeong, S.K. Kim, C. Rohde and S. Choi, *J. Appl. Phys.* **2005**, *98*, 033715.

[134] M.J. Rozenberg, I.H. Inoue, M.J. Sanchez, *Phys. Rev. Lett.* **2004**, *92*, 178302.

[135] M. Quintero, P. Levy, A.G. Leyva and M.J. Rozenberg, *Phys. Rev. Lett.* **2007**, *98*, 116601.

[136] A. Odagawa, Y. Katoh, Y. Kanzawa, Z. Wei and T. Mikawa, *Appl. Phys. Lett.* **2007**, *91*, 133503.

[137] D.L.A. de Faria, S.V. Silva and M.T. de Oliveira, *J. of Raman Spectroscopy* **1997**, *28*, 873.

[138] D. Tsiplakides and C.G. Vayenas, *J. Electrochem. Soc.* **2001**, *148*, E189.

[139] A. Sawa, T. Fujii, M. Kawasaki and Y. Tokura, *Appl. Phys. Lett.* **2004**, *85*, 4073.

VITA

Samantha Glen Matthews was born in Cape Girardeau, MO. In May 2008, she received her Bachelor of Science in Physics with honors from the University of Missouri-Rolla. She received her M.S. degree in Materials Science & Engineering from the Missouri University of Science and Technology in December 2010.